Acta metall. mater. Vol. 39, No. 7, pp. 1469–1480, 1991
Printed in Great Britain.

0956-7151/91 $3.00 + 0.00

COMPUTER SIMULATION OF THE STRUCTURE AND MOBILITY OF TWINNING DISCLOCATIONS IN H.C.P. METALS

A. SERRA[1], R.C. POND[2] and D. J. BACON[2]

[1]Department de Matemàtica Aplicada III, Universitat Politècnica de Cátalunya, ETSE Camins, Jordi Girona Salgado 31, 08034 Barcelona, Spain and [2]Department of Materials Science and Engineering, University of Liverpool, P.O. Box 147, Liverpool L69 3BX, England

(Received 4 April 1990; in revised form 20 December 1990)

Abstract—The properties of twinning dislocations in $[10\bar{1}1]$, $\{10\bar{1}2\}$, $\{11\bar{2}1\}$ and $\{11\bar{2}2\}$ twin boundaries in hexagonal-close-packed metals have been investigated by atomic-scale computer simulation. Care has been exercised (by use of the concept of bicrystal structure maps) to ensure that all possible stable interface structures have been modelled and the work extends the research reported earlier by us [6] in several ways. First, we have now treated the important case of the $\{10\bar{1}1\}$ twin. Second, the dependence of dislocation energy on the atomic structure of the core has been investigated. Third, the mobility of these interfacial dislocations has been examined by computing the critical resolved shear strain for glide. It has been found that the twinning dislocations corresponding to the $\{10\bar{1}2\}$ and $\{11\bar{2}1\}$ twins observed in practice are highly glissile, wheras those for the $\{10\bar{1}1\}$ and $\{11\bar{2}2\}$ modes are not. These effects are deduced to be related to the atomic structure of the core (and, in particular, to its width rather than height), and are found to be consistent with the nature of deformation twinning reported for the h.c.p. metals. For $\{10\bar{1}1\}$ twinning, however, the dislocation of lowest energy and highest mobility does not correspond to the mode observed in practice, implying that twin nucleation may possibly be a controlling factor in that case.

Résumé—On étudie les propriétés des dislocations de macle dans les joints de macle $\{10\bar{1}1\}$, $\{10\bar{1}2\}$, $\{11\bar{2}1\}$ et $\{11\bar{2}2\}$ dans des métaux hexagonaux compacts par simulation numérique à l'échelle atomique. On veille (en utilisant le concept de cartes de structure du bicristal) à s'assurer de ce que toutes les structures d'interface stables possibles soient modélisées et ce travail développe des recherches déja publiées par notre équipe [6] de différentes façons. D'abord, nous traitons le cas important de la macle $\{10\bar{1}1\}$. En second lieu, on étudie la dépendance de l'énergie des dislocations vis à vis de la structure atomique de coeur. En troisième lieu, on examine la mobilité des dislocations interfaciales en calculant la cission réduite pour le glissement. On trouve que les dislocations de macle correspondant aux macles $\{10\bar{1}2\}$ et $\{11\bar{2}1\}$ observées en pratique sont très glissiles, tandis que celles qui correspondent aux macles $\{10\bar{1}2\}$ et $\{11\bar{2}2\}$ ne le sont pas. On trouve que ces effets sont liés à la structure atomique de coeur (et en particulier à sa largeur plutôt qu'à sa hauteur) et sont en accord avec la nature de la déformation par maclage observée dans les métaux hc. Pour le maclage $\{10\bar{1}1\}$ cependant la dislocation de plus basse énergie et de plus forte mobilité ne correspond pas au mode observé en pratique, ce qui implique que la germination de la macle peut être dans ce cas un facteur de contrôle.

Zusammenfassung—Die Eigenschaften der zwillingsbildenden Versetzungen in $\{10\bar{1}1\}$-, $\{10\bar{1}2\}$-, $\{11\bar{2}1\}$- und $\{11\bar{2}2\}$-Zwillingsgrenzen von hexagonal dichtest gepackten Metallen werden mit Computersimulationen im atomaren Maßstab untersucht. Alle möglichen stabilen Grenzflächenstrukturen werden sorgfältig (unter Nutzung des Konzeptes von Bikristallstruktur-Karten) modelliert; diese Arbeit erweitert die früher von uns vorgelegten Untersuchung [6] in mehrfacher Hinsicht. Erstens haben wir jetzt den wichtigen Fall des $\{10\bar{1}1\}$-Zwillings untersucht. Zweitens wird die Abhängigkeit der Versetzungsenergie von der atomaren Struktur des Kernes behandelt. Drittens wird die Beweglichkeit dieser Grenzflächenversetzungen durch die Berechnung der kritischen Scherspannung für Gleitung ermittelt. Es ergibt sich, daß die Zwillingsversetzungen entsprechend den tatsächlich beobachteten $\{10\bar{1}2\}$- und $\{11\bar{2}1\}$-Zwillingen höchst gleitfähig sind, dagegen die der $\{10\bar{1}1\}$- und $\{11\bar{2}2\}$-Zwillige nicht. Diese Effekte werden der atomaren Kernstruktur (und insbesondere deren Breite und nicht deren Höhe) zugeschrieben: sie sind auch mit der für hexagonal dichtest gepackte Metalle berichteten Natur der Bildung von Verformungszwillingen verträglich. Bei $\{10\bar{1}1\}$-Zwillingen allerdings entsprechen die Versetzungen niedrigster Energie und höchster Beweglichkeit nicht der Beobachtung, was darauf hinweist, daß die Zwillings-Keimbildung möglicherweise in diesem Fall der kontrollierende Faktor ist.

1. INTRODUCTION

The atomic structure and other properties associated with interfaces and interfacial defects are of fundamental importance for mechanisms underlying a wide range of phenomena in engineering materials. This is particularly the case in the hexagonal-close-packed (h.c.p.) metals where, in addition to the usual interface-related processes such as creep, segregation and crack nucleation, the formation and mobility of twin boundaries plays a crucial role in polycrystalline ductility (see, for example, the review by Yoo [1]).

The importance of this led to a spate of experimental studies in the 1950s and 60s into the characteristics of deformation twinning in the h.c.p. metals, and the data obtained (see reviews [2, 3]), together with development of the classical crystallographic theory of twinning (e.g. [4]), provided the understanding appraised in [1]. However, the research was unable to account for the different modes of behaviour exhibited by different metals, for these are determined by the atomic nature of the twinning process, and were not understood. As a step in this direction, we have initiated a study using atomic-scale computer simulation to investigate the structure of twin boundaries and the core behaviour of dislocations that can reside in them. In previous papers, we have modelled the structure and dilatation of dislocation-free interfaces of the $\{10\bar{1}2\}$, $\{11\bar{2}1\}$ and $\{11\bar{2}2\}$ twins [5], and examined the core structure of the twinning dislocations (or steps) which, under the influence of the twinning shear stress, cause these twins to expand or contract [6]. We extend this work in the present paper by considering (a) the structure of the $\{10\bar{1}1\}$ twin interface and twinning dislocations, and (b) the ease of movement of twinning dislocations in all four twins under an external shear stress. These are important aspects because $\{10\bar{1}1\}$ twinning is a major component of deformation in some metals under compression parallel to the [0001] (or **c**) axis, and the movement of twinning dislocations controls twin growth.

It should be noted at the outset that the modelling in this programme of research does not attempt to simulate specific h.c.p. metals. The interatomic potentials used, like those employed in the main for the work reported to date on cubic metals, are pair potentials. They are the best available, but are incapable of mimicking the wide range of bonding types, and hence the wide range of physical properties, exhibited by the real h.c.p. metals. They simply describe model h.c.p. crystals with two-body bonding and c/a lattice parameter ratios close to ideal ($=1.633$). We shall return to this point later. First, in Section 2 we briefly outline the crystallographic parameters and computational procedures used. Then, in Sections 3 and 4, results are presented for topics (a) and (b) referred to above. Finally, these results are discussed in Section 5 and summarised in section 6.

2. PROCEDURE

The crystallography of the dislocations considered here and in [6] was derived from the general treatment of Pond [7], who showed that admissible interfacial defects are characterised by combinations of a symmetry operation from each of the two adjacent crystals. Three distinct classes of dislocation can occur in this way, as follows.

(i) Class 1: arises from broken translation symmetry when the bicrystal is formed, i.e. the Burgers vector **b** is simply the difference betweeen translation vectors of the two half crystals.

(ii) Class 2: arises when mirror planes or rotation axes of the half crystal are aligned, but the intrinsic glide components are either unequal or not parallel.

(iii) Class 3: arises when operations such as mirrors or mirror-glide elements are coincident in the bicrystal but can be broken by a rigid-body displacement.

Steps may be associated with the cores of these interfacial defects [7].

For the $(10\bar{1}1)$ twin, the maximum possible symmetry (exhibited by *unrelaxed* atomic positions) is shown schematically in Fig. 2 of [9], which complements equivalent sketches for the other three twins given in Fig. 2 of [6]. For the $(10\bar{1}1)$ twin, the upper and lower crystals are related by a 2-fold axis parallel to the interface and mirror symmetry across it. Furthermore, the $(1\bar{2}10)$ mirror plane is coincident in both crystals and the bicrystal exhibits this symmetry. Thus, in the light of the foregoing statements, and taking results from the other three twins from [6], the classes of dislocation that can exist in principle in the twin boundaries commonly found in the h.c.p. metals are

$(10\bar{1}1)$: class 1, 3
$(10\bar{1}2)$: class 1, 3
$(11\bar{2}1)$: class 1, 2, 3
$(11\bar{2}2)$: class 1, 3.

The class 1 dislocations are the twinning dislocations of the Bravais lattice, but, as revealed by the computer simulations in [6], it is possible for a class 1 dislocation to decompose into two class 2 lines for the $(11\bar{2}1)$ twin, and each of these is a twinning dislocation for this boundary in the h.c.p. structure.

In theory, an infinite number of Burgers vectors **b** can be defined as above for a given interface plane: in practice, actual twinning dislocations may be expected to have small magnitude of **b** and small height of the steps they form on the interface. Also, a deformation twin of a given habit plane is generally observed to correspond to a characteristic twinning shear (in both direction and magnitude), and this implies a characteristic twinning dislocation (both in sign and magnitude of **b**). As a result of these factors, the parameters that define the class 1 twinning dislocations of possible interest for the $(11\bar{2}1)$, $(11\bar{2}2)$ and $(10\bar{1}2)$ twins were presented in Table 1 of [6]. To complete this, we provide here the parameters for possible $(10\bar{1}1)$ modes, as listed in Table 1 of the present work. **n** is the unit vector normal to the twin plane K_1, $\mathbf{t}(\mu)$ and $\mathbf{t}(\lambda)$ are the translation vectors (of the lower and upper crystals) whose difference gives **b**, h is the step height in units of the spacing $d(K_1)$ of the K_1 planes of the Bravais lattice, s is the magnitude b/h of the twin-

ning shear, η_1 is the twinning direction, and K_2 and η_2 are the conjugate twinning plane and direction respectively. It can be seen that we have considered three possible dislocations for $(10\bar{1}1)$ twinning, the reasons for which will be discussed presently. As a general notation to provide easy identification, we shall add a subscript h to **b** to denote the step height. Thus, we consider dislocations $\mathbf{b}_2$, $\mathbf{b}_3$ and $\mathbf{b}_4$ for $(10\bar{1}1)$, dislocation $\mathbf{b}_2$ for $(10\bar{1}2)$, dislocation $\mathbf{b}_{1/2}$ for $(11\bar{2}1)$, and dislocations $\mathbf{b}_1$ and $\mathbf{b}_3$ for $(11\bar{2}2)$. (For full details of the last three twin planes, see Table 1 of [6]).

It is important when simulating periodic two-dimensional interfaces in crystals to ensure that all possible interfacial structures are sampled in the computing procedure. In crystals with a single-atom basis, this requires that all distinct rigid-body translations of one crystal parallel to the surface of the other be considered prior to atomic relaxation. The Wigner–Seitz cell of such translations has been termed the "cell of non-identical displacements" (C.N.I.D.) [8]. For crystals with more than one atom per lattice site, however, more than one C.N.I.D. may exist for a given interface orientation, and in that case a structure represented by a point on one C.N.I.D. cannot be obtained from a structure given by a point on another C.N.I.D. by a rigid-body displacement alone. This is discussed in detail in [9]. The result is that the number of C.N.I.D.s for the four twins $(10\bar{1}1)$, $(10\bar{1}2)$, $(11\bar{2}1)$ and $(11\bar{2}2)$ is 4, 4, 4 and 1 respectively. However, for a given interface orientation, the symmetry elements present may result in two bicrystals represented by points on two distinct C.N.I.D.s being crystallographically equivalent (and energetically degenerate). Thus, there are three distinct C.N.I.D.s for the $(10\bar{1}1)$ twin, three for the $(10\bar{1}2)$ and two for the $(11\bar{2}1)$. (Two of those for $(10\bar{1}2)$ were omitted in [5] and [6], and the full set is given in [9].) We have therefore considered relaxed atomic structures generated by translations in all these distinct C.N.I.D.s for the present work. For the $(10\bar{1}2)$ interface, which was not considered fully previously [5, 6], no new structures of low energy were found.

The computational procedure used in [6] has been adopted again here. One pair-potential has been employed in the main: it is the oscillatory potential called na56 in [6]. It gives $c/a = 1.619$ for a stable perfect crystal, and has been shown in studies of point [10], line [11] and planar [5, 6] defects to be superior to others for the h.c.p. stucture. Unlike our previous study [6], only dislocations in the edge orientation have been considered in the present work. A model of a twinned crystal containing a twinning dislocation in this orientation is shown schematically in Fig. 1. The maximum number x and z *lattice* planes in the inner region of relaxable atoms of the model was 70 and 29 for $(10\bar{1}1)$, 80 and 21 for $(10\bar{1}2)$, 208 and 27 for $(11\bar{2}1)$, 136 and 35 for $(11\bar{2}2)$. Neither the core structure nor movement of twinning dislocations was

Table 1. Twinning dislocation parameters for $(10\bar{1}1)$ twins $\left(K_1 = (10\bar{1}1),\ \mathbf{n} = \frac{\Lambda}{(2\Lambda^2+1)^{1/2}}[\bar{1}01],\ \Lambda = \left(\frac{2}{3}\right)^{1/2}\frac{c}{a}\right.$ and $|\mathbf{b}|$ is in units of $\left.\left(\frac{3}{2}\right)^{1/2} a\right)$

Dislocation	η_1	$\mathbf{t}(\Lambda)$	$\mathbf{t}(\mu)$	$\mathbf{b}$	$\lvert\mathbf{b}\rvert$	$h/d(K_1)$	$s = \lvert\mathbf{b}\rvert/h$	K_2	η_2
$\mathbf{b}_2$	$[13\,\bar{4}\bar{1}\,28\,15]$	$[10\bar{1}0]$	$\frac{1}{3}[\bar{2}11\bar{3}]$	$\frac{1}{123}[13\,\bar{4}\bar{1}\,28\,15]$	0.448	+2	0.358	$(\bar{1}6\bar{5}\bar{3})$	$[5\bar{1}\bar{4}3]$
$\mathbf{b}_3$	$[10\bar{1}2]$	$(\bar{1}01\bar{1})$	$[10\bar{1}1]$	$\frac{(2\Lambda^2-2)}{(2\Lambda^2+1)}[\bar{1}012]$	$\frac{2^{1/2}(2\Lambda^2-2)}{(2\Lambda^2+1)^{1/2}}$	+3	$\frac{2^{1/2}(2\Lambda^2-2)}{3\Lambda}$	$(10\bar{1}\bar{2})$	$[\bar{1}01\bar{1}]$
$\mathbf{b}_4$	$[10\bar{1}\bar{2}]$	$\frac{1}{3}[\bar{5}14\bar{3}]$	$\frac{1}{3}[\bar{4}15\bar{3}]$	$\frac{(2\Lambda^2-3)}{(2\Lambda^2+1)}[\bar{1}012]$	$\frac{2^{1/2}(2\Lambda^2-3)}{(2\Lambda^2+1)^{1/2}}$	+4	$\frac{2^{1/2}(2\Lambda^2-3)}{4\Lambda}$	$(10\bar{1}\bar{3})$	$[30\bar{3}2]$

Note: The entries for η_1, $\mathbf{b}$, $|\mathbf{b}|$, s and K_2 under $\mathbf{b}_2$ are for the special case of ideal c/a, i.e. $\Lambda^2 = 16/9$. For the general case, the following apply,
$\eta_1 = [(5-2\Lambda^2),\ -(2\Lambda^2+1),\ 4(\Lambda^2-1),\ 3(2\Lambda^2-3)]$

$$\mathbf{b} = \frac{1}{3(2\Lambda^2+1)}\eta_1$$

$$|\mathbf{b}| = \frac{(14+11\Lambda^2-28\Lambda^4+12\Lambda^6)^{1/2}}{3^{1/2}(1+2\Lambda^2)}$$

$$s = \frac{(14+11\Lambda^2-28\Lambda^4+12\Lambda^6)^{1/2}}{4\Lambda 3^{1/2}(1+2\Lambda^2)^{1/2}}$$

$$K_2 = [(-6-9\Lambda^2+6\Lambda^4),\ (4+8\Lambda^2),\ (2+\Lambda^2-6\Lambda^4),\ (14+19\Lambda^2-18\Lambda^4)].$$

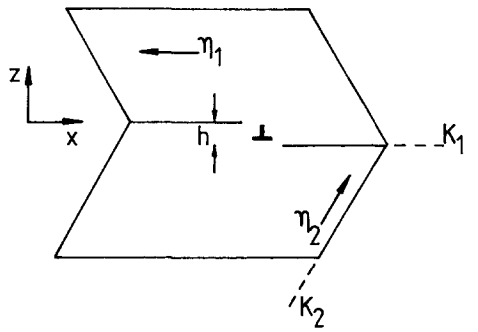

Fig. 1. Schematic illustration of a twinned crystal showing the twinning elements K_1, η_1, K_2 and η_2, and the interfacial step associated with a twinning dislocation.

found to be sensitive to model size for the numbers indicated. Periodic boundary conditions were imposed in the y direction parallel to the dislocation line.

External shear strain $e(=e_{xz})$ was applied via a simple shear displacement of all atoms in the model. Starting from an "unstrained" ($e = 0$) relaxed crystal, strain was imposed in small increments of ± 0.001, with atomic relaxation to minimise the potential energy allowed after each increment. The critical strain e_c for free movement of the twinning dislocation along an interface was taken to be that for which displacement of the centre of the dislocation core occurred over one periodic repeat distance of the lattice in the $\pm x$ direction.

3. (10$\bar{1}$1) TWIN

3.1. Dislocation-free interface

The stable dislocation-free interface of lowest energy is shown in the [1$\bar{2}$10] projection of relaxed atomic positions in Fig. 2(a). (Its unrelaxed state was the structure in Fig. 2(c) of [9]). The relaxed boundary is defined by a single plane of atoms, formed by the movement and subsequent coalescence of two planes of atoms which were distinct in the unrelaxed bicrystal. The atoms in this interface experience alternating tensile/compressive hydrostatic stress [$p = -\frac{1}{3}(\sigma_{xx} + \sigma_{yy} + \sigma_{zz})$], as shown by the arrows in the left half of the figure. (For the scale mark for p at the bottom left, the energy unit ϵ is the approximate depth of the pair potential at the nearest neighbour spacing and Ω is the volume per atom. For purposes of comparison, the bulk modulus of an na56 crystal is $64\,\epsilon/\Omega$.) The shear stress component σ_{xz}, on the other hand, is negligible at the interface plane, and alternates in sign along the atoms in the two adjacent planes, as shown by the arrows in the right half of the figure. This behaviour with regard to p and σ_{xz} is very similar to that of the (10$\bar{1}$2) twin using the same potential [5, 6], and, furthermore, the volume change associated with the interface, as measured by the relative z displacement of the x–y boundaries of the outer fixed region of the model, is the same, namely $+0.004\,a$. The twin boundary energy γ_T for the (10$\bar{1}$1) twin, in units of ϵ/a^2, is given in Table 2, together with γ_T values for the other three twins taken from [5]. (The results in [5] were based on a value of a which was about 9% too large: they are corrected here.) There is no obvious correlation between γ_T and structural features of a boundary.

Other stable boundaries were sought, based on the other two C.N.I.D.s in Fig. 2(d) and (e) of [9]. Two stable configurations of high γ_T were found: they correspond to that in Fig. 2(a) with rows of vacancies either in the interface, or in a plane adjacent to the interface. The former is plotted in [1$\bar{2}$10] projection, together with a map of pressure p, in Fig. 2(b) and has $\gamma_T = 2.73\,\epsilon/a^2$, i.e. about four times that of the low-energy structure. These "well-packed" and "open" boundary structures are similar to the two (11$\bar{2}$1) configurations presented in [5]. Likewise, stable "open" structures exist, but have high energy, for the (10$\bar{1}$2) twin. In the following we consider only the boundaries of lowest energy.

3.2. (10$\bar{1}$1) twinning dislocations

As explained in Section 1, the Burgers vectors of possible twinning dislocations in the (10$\bar{1}$1) twin boundary are defined by considering the differences between translation vectors of the lower and upper lattices, expressed in the coordinate frame of one of them. The step height of such a dislocation is one half of the scalar product of the unit vector normal to the boundary with the sum of the two translation vectors. When the possibilities are assessed in this way, it is found that the dislocations with $h = d(K_1)$ and $2d(K_1)$ do not correspond to the [10$\bar{1}\bar{2}$] direction η_1

Table 2. Twin boundary energy and dislocation parameters and properties

Twin	γ_T	**b**	s	b^2/a^{2*}	$h/d(K_1)$	Line energy	Elastic energy	Core energy	Core width	e_c
(10$\bar{1}$1)	$0.64\,\epsilon/a^2$	$\mathbf{b}_2$	0.36	$\frac{2}{7}$	2	$3.6\,\epsilon/a$	$2.4\,\epsilon/a$	$1.2\,\epsilon/a$	Narrow ($\sim 2a$)	± 0.006
		$\mathbf{b}_3$	0.55	$\frac{196}{123}$	3	25.4	17.8	7.6	Narrow ($\sim a$)	—
		$\mathbf{b}_4$	0.15	$\frac{25}{123}$	4	4.0	2.3	1.7	Narrow ($\sim a$)	± 0.02
(10$\bar{1}$2)	1.15	$\mathbf{b}_2$	0.12	$\frac{1}{51}$	2	0.1	0.1	0.0	Wide ($\sim 6a$)	± 0.002
(11$\bar{2}$1)	0.73	$\mathbf{b}_{1/2}$	0.61	$\frac{3}{140}$	$\frac{1}{2}$	0.3	0.3	0.0	Wide ($11a$)	± 0.001
(11$\bar{2}$2)	0.92	$\mathbf{b}_1$	1.22	$\frac{3}{11}$	1	3.1	3.0	0.1	Wide ($\sim 4a$)	± 0.002
		$\mathbf{b}_3$	0.27	$\frac{4}{33}$	3	3.7	1.6	2.1	Narrow ($\sim a$)	$+0.014$
		$\mathbf{b}_4$	0.10	$\frac{1}{33}$	4	4.1	0.4	3.7	Narrow ($\sim a$)	>0.04

*For the case $c/a = \sqrt{8/3}$.

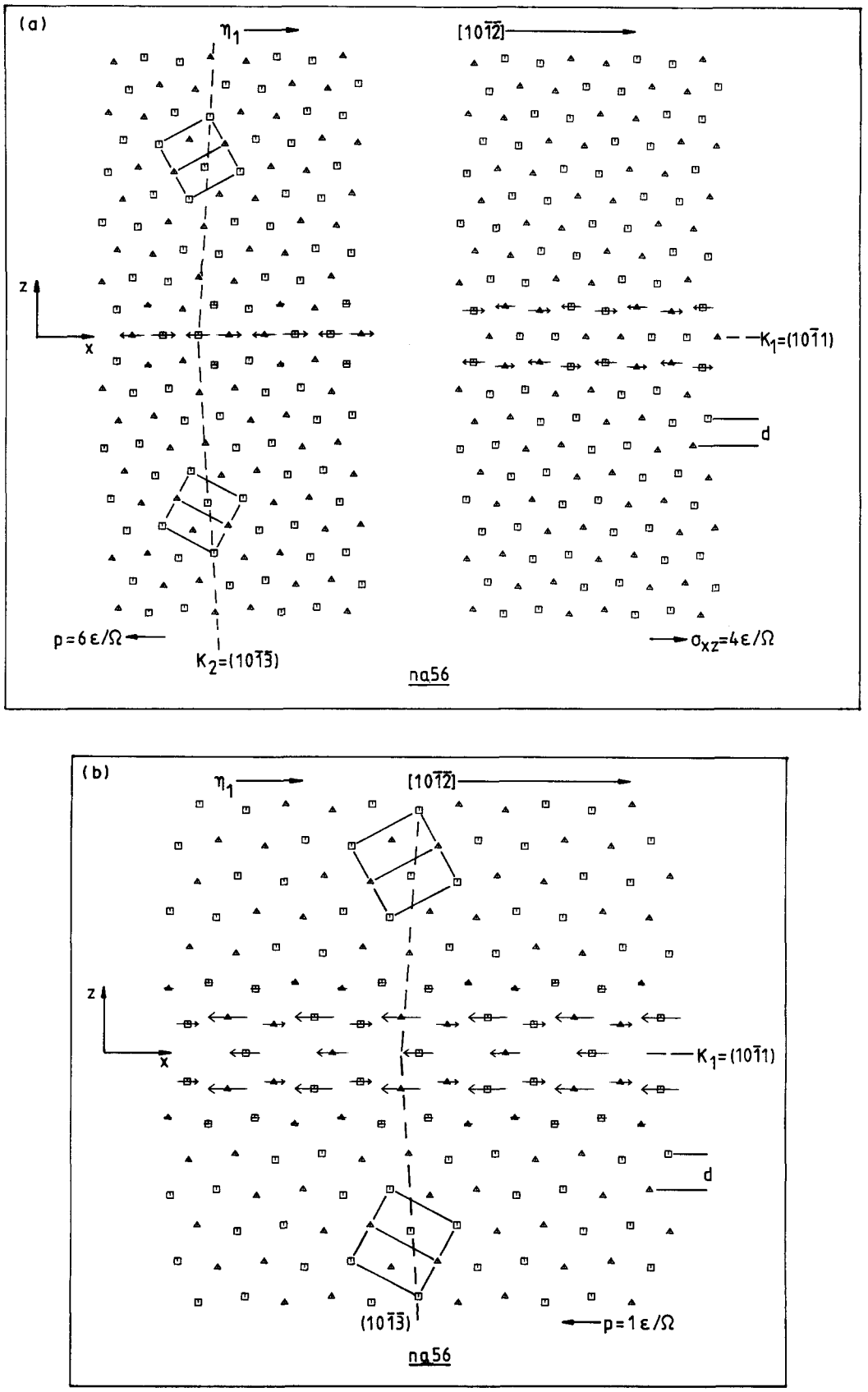

Fig. 2. $[\bar{1}2\bar{1}0]$ projections of the relaxed structure of two stable, dislocation-free $(10\bar{1}1)$ twin boundaries. The interface in (a) has the lower energy.

of the twinning shear observed experimentally. The dislocations denoted $\mathbf{b}_3$ and $\mathbf{b}_4$ in Table 1 have the correct sense of η_1, but steps of height $3d(K_1)$ and $4d(K_1)$ respectively. For a crystal of near-ideal c/a ratio, $\mathbf{b}_3$ and $\mathbf{b}_4$ are approximately $\frac{14}{41}[10\bar{1}\bar{2}]$ and $\frac{5}{41}[10\bar{1}\bar{2}]$ respectively. The vector $\mathbf{b}_4$, which has the smaller magnitude but larger step, corresponds to the twinning elements found in practice. Nevertheless, the core structure of both dislocations has been simulated here.

As in the computational procedure adopted in [6] for the $(11\bar{2}2)$ twin dislocations with $h = 3d(K_1)$ and $4d(K_1)$, the unrelaxed dislocation was created in a previously-relaxed planar boundary by imposing the displacement field of a dislocation according to linear, isotropic elasticity. This displaces atoms of the

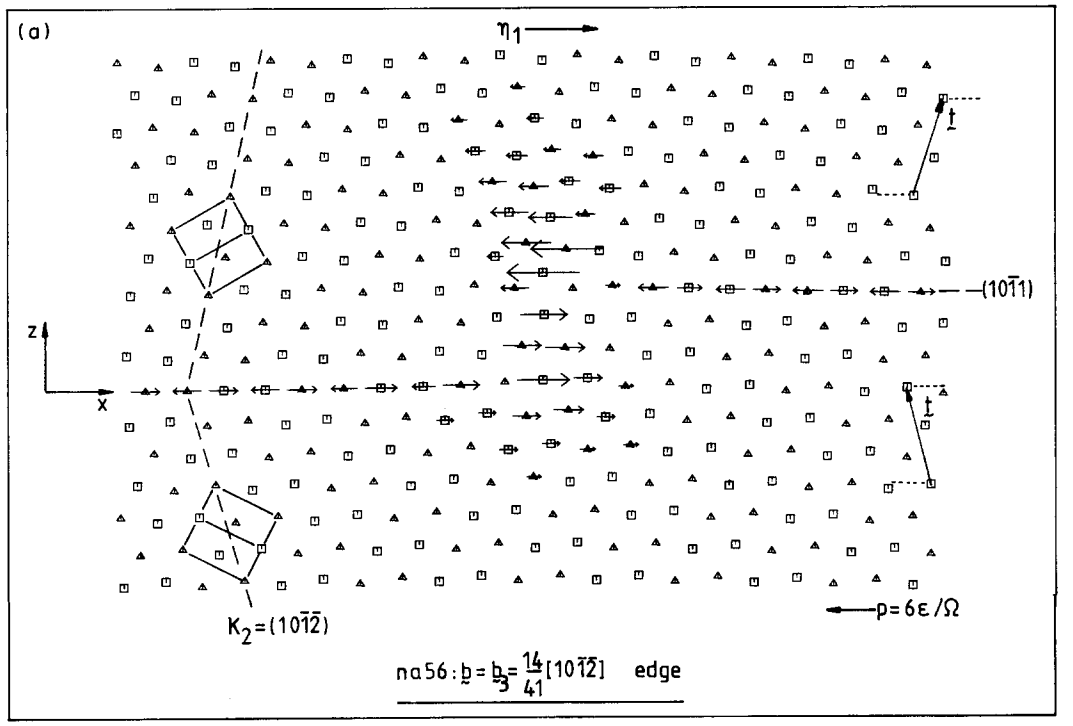

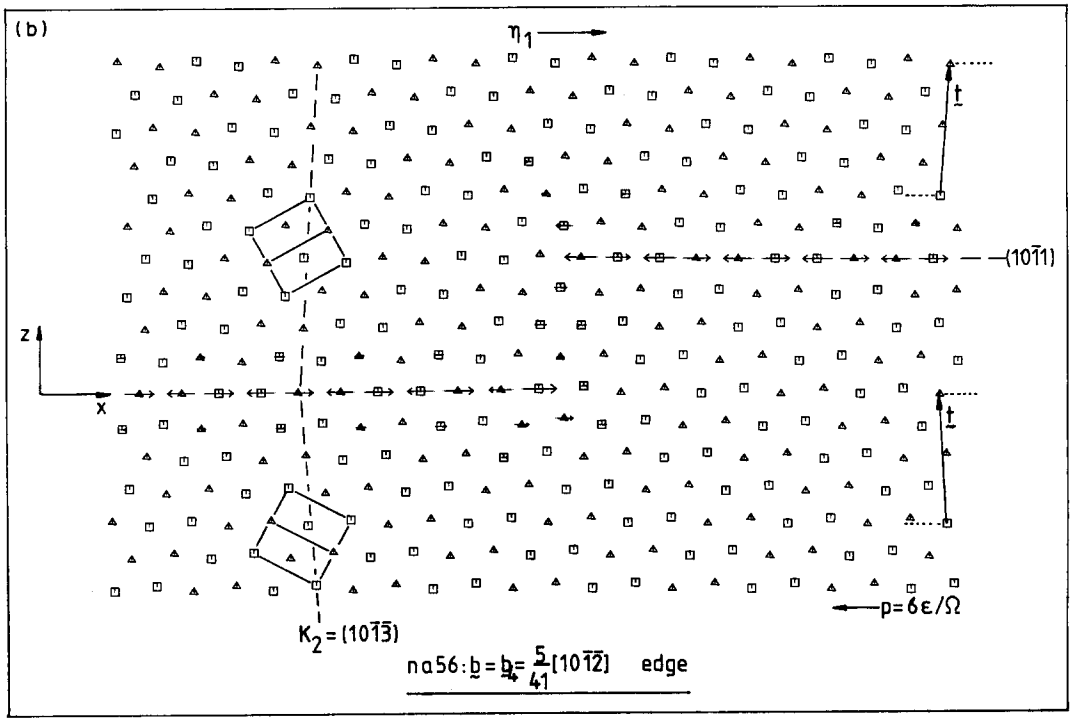

Fig. 3. *Continued on facing page.*

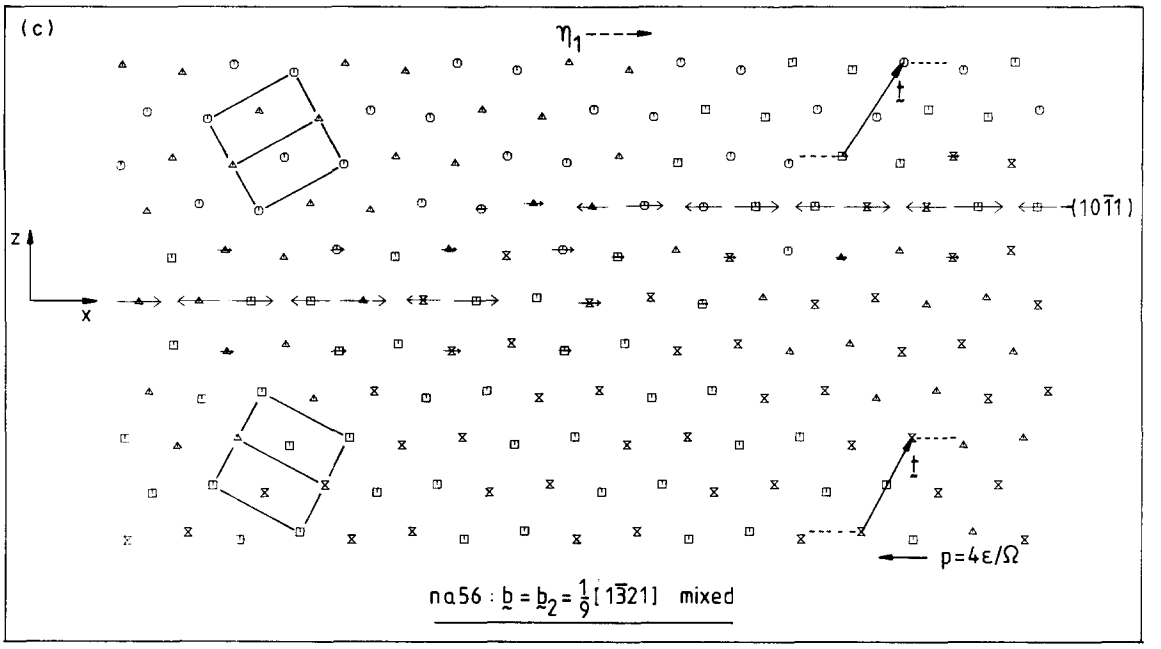

Fig. 3. Relaxed atomic structure around the cores of (a) the $\mathbf{b}_3$ dislocation, (b) the $\mathbf{b}_4$ dislocation, and (c) the $\mathbf{b}_2$ dislocation in the $(10\bar{1}1)$ twin interface.

third (or fourth) lattice plane from the interface of the upper crystal to near their correct new sites in the lower crystal: atoms in the two (or three) intervening planes have to move individually to restore the h.c.p. structure of the lower crystal. These individual shuffles are not unique—see [6] for more detail—and the results presented here are those for the cores with lowest distortion and energy.

The relaxed core structures of the $\mathbf{b}_3$ and $\mathbf{b}_4$ dislocations are plotted in $[1\bar{2}10]$ projection in Fig. 3(a) and (b) respectively. Also indicated on these figures are the projections of an h.c.p. unit cell in each crystal, the direction and trace of η_1 and K_2, and the projections of the translation vectors $\mathbf{t}$ used to generate $\mathbf{b}$ and h. The stress maps denoting hydrostatic pressure p show clearly that the dislocations cause the boundary to step up in traversing from left to right. (This is the reverse of the situation drawn in Fig. 1 since η_1 is reversed.) They also indicate that both cores are highly localised in a region an atom-spacing or so wide in the x direction. Atomic displacements parallel to the dislocation line were negligible ($<0.01a$). Despite having the lower step height, the $\mathbf{b}_3$ dislocation has a much higher energy than $\mathbf{b}_4$, reflecting the highly stressed state of its core configuration. The dislocation energy, taken as the extra bicrystal energy introduced by the presence of the line divided by its length, is given in Table 2, together with values for some of the dislocations simulated in [6]. As they stand, line energies for *different* twins in this Table are not strictly comparable since they depend on the crystal dimensions in the x–z plane, which are not constant. This will be returned to in Section 5.

We should remark that another $(10\bar{1}1)$ twinning dislocation, with Burgers vector denoted by $\mathbf{b}_2$, has also been considered here. It is included in Tables 1 and 2, although it does not have the η_1 specified above. We shall return to a fuller description of it in Section 5.

4. MOVEMENT UNDER APPLIED STRAIN

For this part of the study, we have considered all the dislocations listed in Table 2, applying a shear $\pm e_{xz}$ in each case to induce the dislocation to move right/left along the interface: this causes the upper crystal to grow at the expense of the lower, or shrink, depending on the direction of η_1. The relaxed core structure for the two $(10\bar{1}1)$ defects were shown in Fig 3(a) and (b), and those for four of the other five cases are reproduced from [6] in Fig. 4(a)–(d). (That for the $\mathbf{b}_4$ dislocation in the $(11\bar{2}2)$ twin (Fig. 12 of [6]) is omitted in the interests of space.) It has been found that some of the dislocations move easily at low values of the critical strain e_c, while the others are almost sessile and require high strains to be applied before movement occurs. The former group is considered first.

The positive edge dislocation in the $(11\bar{2}1)$ boundary in Fig. 4(b) moves at the lowest strains applied in our simulations, i.e. to the right/left when e_{xz} equals ± 0.001. The characteristic feature of this class 2 dislocation is its very wide core, which, as seen from the figure, spreads over the breadth of the interface in the relaxable region of the model. The width of this planar core, defined by the length over which the core disregistry increases from $b/4$ to $3b/4$, is $11a$, which is approximately $75b$. (The screw core is also very

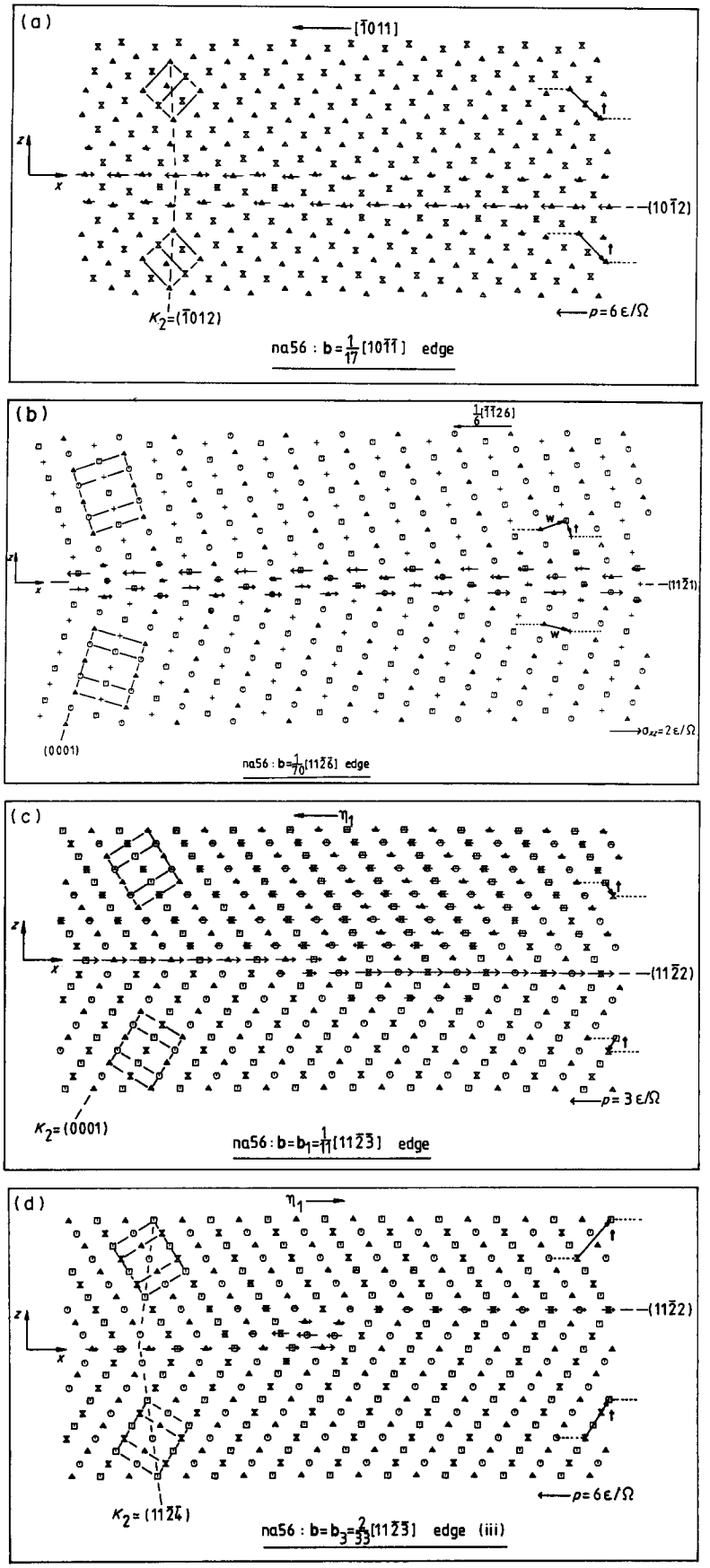

Fig. 4. Relaxed atomic structure around the cores of (a) the $\mathbf{b}_2$ dislocation in the (10$\bar{1}$2) twin, (b) the $\mathbf{b}_{1/2}$ dislocation in the (11$\bar{2}$1) twin, (c) the $\mathbf{b}_1$ dislocation in the (11$\bar{2}$2) twin, and (d) the $\mathbf{b}_3$ dislocation in the (11$\bar{2}$2) twin.

wide–see Fig. 8(b) of [6]–and this also glides at $e_{xz} = \pm 0.001$.) We believe that e_c is low for this twinning dislocation because the core is planar and wide, and no atomic shuffles are required to move atoms to the correct sites in their new crystal as the dislocation glides past, i.e. correct structure is obtained by the relative displacement **b** alone. The core of the $\mathbf{b}_1$ dislocation in the $(11\bar{2}2)$ twin shown in Fig. 4(c) has a slighly higher h and narrower core width ($\sim 4a$), but basically meets the same criteria, and, indeed, we find that it moves to the right/left at e_c values of ± 0.002. The step for the positive edge dislocation in the $(10\bar{1}2)$ interface in Fig. 4(a) has a greater height, but, nonetheless, the core is distinctly planar and has a width as defined above of about $6a$. Furthermore, although some shuffles are required to restore the correct position to each atom as the interface moves up or down, they are very small. As can be seen from Fig. 4(a), atoms in planes highlighted by the p arrows undergo small z displacements, and atoms in the two atomic planes in between experience only small x displacements, which alternate in sign from atom to atom. Consequently, e_c was found to be only ± 0.002 for movement to the right/left. All these results are summarised in Table 2.

Of the other dislocations, that with $\mathbf{b}_3$ in the $(11\bar{2}2)$ twin has been treated most thoroughly. As can be seen for the positive edge dislocation in Fig. 4(d), the core, like that of the $(10\bar{1}1)$ dislocations in Fig. 3, is both localised and three-dimensional. Initially, simulations were undertaken with a relaxable inner region containing 25 atomic $(11\bar{2}2)$ planes, but no movement of the line was found to occur even for $|e_{xz}|$ values as large as 0.04. When thicker crystals containing more planes were considered, movement to the right was observed at $e_{xz} = 0.016$ for 31 planes and 0.014 for 35 planes. This movement required small shuffles in the x direction and much larger shuffles in the y direction of atoms in the two intermediate planes of the interface step. With reference to the alternating sequence of atoms along the x rows of projected positions in Fig. 4(d), it is clear that pairs of atoms denoted ○ and △ on adjacent $(11\bar{2}2)$ planes have to be displaced respectively to × and □ sites, and vice versa, as the dislocation moves. In view of the dependence of e_c on block thickness, the influence of a normal strain e_{zz} applied simultaneously with e_{xz} was investigated for a model with 31 x–y planes of atoms. As e_{zz} took the sequence $+0.002$, $+0.001$, 0, -0.001 and -0.002, e_c was found to have the values 0.018, 0.018, 0.016, 0.014 and 0.018. Thus, the reduction brought about by a small compressive stress is itself small.

It should be noted that in none of these computer experiments could the dislocation be induced to glide to the left under negative e_{xz} values. Attempts were also made to assist such movement by imposing small y displacements, consistent with the shuffles described above, to atoms in the core before relaxation. This had no effect on e_c except when the displacements were sufficiently large ($\pm a/2\sqrt{3}$) to produce the site exchanges ○ to × and △ to □, and then dislocation movement to the left occurred at $e_{xz} = 0.02$. Even so, it was not sustained unless the reverse shuffles × to ○ and □ to △ were also artificially imposed.

In addition to the core configuration considered above, alternative core structures of higher energy, such as those labelled $\mathbf{b}_3$(i) and $\mathbf{b}_3$(ii) in [6], were investigated, but their mobility was even lower. We conclude, therefore, that the $\mathbf{b}_3$ twinning dislocation is much less glissile than the $\mathbf{b}_1$ dislocation in the same boundary, and has a mobility which is asymmetric with respect to the direction of the twinning shear. The $\mathbf{b}_4$ dislocation of the $(11\bar{2}2)$ twin (see Fig. 12 of [6]) was not considered in as much detail since its h is even larger and the η_1 direction is the reverse of that found experimentally, i.e. the same as that of the $\mathbf{b}_1$ step. Its glide requires atomic shuffling on three atomic planes, and no movement was produced even when $e_{xz} = \pm 0.04$.

In the light of these results for the $(11\bar{2}2)$ twin, it was anticipated that the $\mathbf{b}_4$ dislocation in the $(10\bar{1}1)$ boundary would be difficult to move, and this proved to be the case. As can be seen from Fig. 3(b), the atoms in a row parallel to the x axis in the projection form an alternating sequence of pairs denoted by symbols △ and □, but this sequence is broken in the three atomic planes which traverse the step of this narrow core. Thus, for the dislocation to move along the interface, shuffles △ to □ to △ of magnitude $a/2$ must occur on three adjacent planes in the core region. Under the influence of a shear strain alone, the dislocation did not move for positive or negative strains of magnitude up to 0.02, irrespective of the z dimension of the computational block or the imposition of small compressive or tensile e_{zz} strains. Movement to the right could be induced by the imposition of core shuffles in the y direction. For example, the core shifted to the right by $\frac{1}{4}[\bar{1}012]$ at $e_{xz} = 0.015$ when shuffles of magnitude $a/3$ were applied and continued to move as the strain was increased further. As was found for the $(11\bar{2}2)$ case, sustained movement to the left could not be obtained in this way.

5. DISCUSSION

The results presented here provide a considerable extension of those of our earlier studies on planar and dislocated interfaces of $(10\bar{1}2)$, $(11\bar{2}1)$ and $(11\bar{2}2)$ twins. First, the bicrystal structure maps known as C.N.I.D.s provide a rigorous procedure for sampling all possible twin interfaces in their unrelaxed state prior to energy minimisation in the computer. This lends confidence to the assertion that the dislocation-free interfaces on which the rest of the modelling is based are stable and not metastable. (In this connection, we note that Hagège *et al.* [12] report a stable variant of the $(10\bar{1}2)$ twin with a plane of atoms at the interface which is faceted rather than flat. We have

been unable to reproduce this, and it is not clear if it arises as a result of the form of the Lennard–Jones potential used.) Second, the results for the $(10\bar{1}1)$ twin show that although the interface structure and stresses are superficially similar to those of the $(10\bar{1}2)$ boundary, the core structures of twinning dislocations in these two twins are distinctly different. The two defects $\mathbf{b}_3$ and $\mathbf{b}_4$ consistent with the observed η_1 for $(10\bar{1}1)$ twinning have cores strongly localised at the (high) steps they create on the boundary. Nevertheless, the dislocation $\mathbf{b}_4$ corresponding to the twinning shear measured experimentally has much the lower energy of the two, despite having a higher value of h. Third, the twinning dislocations simulated in this paper tend to fall into two classes, as implied by the data of Table 2. Either the cores have a planar form distributed along the boundary, in which case the boundary step is very glissile, or the cores are very localised with an abrupt step, in which case the dislocation is relatively sessile. This behaviour is only partly related to the step height, for although h is comparatively large for the $(10\bar{1}2)$ boundary, the twinning dislocation glides easily. The descriptions offered here show that the magnitudes and complexity of the atomic shuffles required as the step traverses the K_1 atomic planes are factors that control core width, and hence mobility.

The structural features are also reflected in the core energy of these interfacial defects, i.e. to that contribution to the dislocation energy associated with the region of the bicrystal within which the displacement of any atom relative to its neighbours is beyond the limit of harmonic behaviour. This region is difficult to define with certainty since sizeable stresses can exist even in a dislocation-free interface. However, semi-quantitative assessment of this problem can be arrived at as follows. The "elastic" contribution to the "total" line energy given in Table 2 may be taken in a first approximation to have the conventional form $[\mu b^2/4\pi(1-\nu)]\ln(R/r_0)$, where μ and ν are the shear modulus and Poisson's ratio respectively (as determined for the na56 potential [11]), and R and r_0 are the outer radius of the computational cell and the dislocation core radius respectively. Various ways may be found for defining r_0, but for simplicity we take $r_0 = h$ and for R set πR^2 equal to the area of relaxable region in the x–z plane; R differs in the present case from twin to twin. The "elastic" and hence "core" terms in the energy estimated in this way for each dislocation are included in Table 2. It is clear that a strong correlation exists between core energy, core width and step mobility. When the step height and/or atomic shuffles are such that the core disregistry can spread over the boundary plane, the contribution of the core energy is very small and the step very glissile. The immobile cores are narrow and their core energy is large, and can even dominate when $|\mathbf{b}|$ is small.

These conclusions prompt the obvious question of how does $\{10\bar{1}1\}$ and $\{11\bar{2}2\}$ twinning occur in real h.c.p. metals, for the dislocations associated with the observed twinning elements have been found difficult to move in our simulations, i.e. $\mathbf{b}_4$ in $(10\bar{1}1)$ and $\mathbf{b}_3$ in $(11\bar{2}2)$. The latter twin is particularly intriguing since the $\mathbf{b}_1$ dislocation, although corresponding to a mode not seen experimentally, is apparently associated with a very mobile step. With regard to this last point, it is clear from Fig. 4(a), (b) and (c) that the $(10\bar{1}2)$, $(11\bar{2}1)$ and $\mathbf{b}_1$ $(11\bar{2}2)$ modes occur under the same general sense of applied load, e.g. tension in the [0001] direction. Thus, although the $\mathbf{b}_1$ dislocation in the $(11\bar{2}2)$ boundary is fairly mobile, this mode may not have the chance to arise in competition with the $(10\bar{1}2)$ and $(11\bar{2}1)$ modes, which have much lower twinning shears and twinning dislocation energies. It should be further noted that the high mobility predicted for the $(11\bar{2}1)$ class 2 twinning dislocation is entirely consistent with large-scale reversible movement of this boundary found to be responsible for mechanical damping in zirconium [13]. The data of Table 2 imply that neither γ_T nor s are paramount in determining the modes of deformation twinning.

The two $(10\bar{1}1)$ modes and $\mathbf{b}_3$ $(11\bar{2}2)$ mode, on the other hand, have twinning directions which relieve loadings in the opposite sense to the other cases, i.e. compression in the [0001] direction, as can be deduced from Fig. 3(a) and (b) and Fig. 4(d). Thus, they do not compete with any modes with very mobile twinning dislocations. The $\mathbf{b}_4$ $(10\bar{1}1)$ and $\mathbf{b}_3$ $(11\bar{2}2)$ modes do occur in practice, as reported for titanium by Paton and Backofen [14] for example. These workers compressed single crystal samples of titanium along the [0001] axis to strains of 5% at temperatures between 25 and 800°C, and found that the strain was almost entirely accommodated by $\{11\bar{2}2\}$ twinnming from 25 to 400°C and in combination by $\{10\bar{1}1\}$ twinning and $\frac{1}{2}\langle 11\bar{2}3\rangle$ slip above 400°C. They deduced that twinning was controlled by a nucleation process for $\{11\bar{2}2\}$ twins and twin boundary propagation for the $\{10\bar{1}1\}$ twins. Furthermore, the latter twins were very thin in shape and the stress for their propagation decreased with increasing temperature. It should be emphasised that these experiments were arranged such that slip could not occur, except at high temperatures. Similar observations with respect to $\{11\bar{2}2\}$ and $\{10\bar{1}1\}$ twinning were reported from [0001] compression experiments of zirconium by Aktar [15]. The results of our computer simulations are therefore generally in accord with these observations in the following respects. First, the propagation of $\{10\bar{1}1\}$ and $\{11\bar{2}2\}$ twins by the glide of twinning dislocations is not easy, and should only be expected when other deformation modes are inoperative. Second, the mobility of twinning dislocations in $\{11\bar{2}2\}$ boundaries is marginally higher than that of those in $\{10\bar{1}1\}$. Third, our simulations mimic conditions at temperature equal to 0 K, and it was noted that the glide of these localised steps is assisted by additional displacements of core atoms. Propagation of these two

boundaries will therefore be thermally activated, i.e. the stress for twin propagation should have a strong temperature-dependence.

We remarked earlier that the $(10\bar{1}1)$ $\mathbf{b}_4$ dislocation corresponds to the correct twinning mode. Experimental verification that this mode occurs was given for magnesium by Reed-Hill [16] and for titanium by Paton and Backofen [14, 17]. For that reason, we did not consider dislocations which give different η_1 directions when starting this research. However, a referee drew out attention to the fact that another $\{10\bar{1}1\}$ mode has been reported in the literature, with $K_1 = (10\bar{1}1)$, $\eta_1 =$ '$[1\bar{3}21]$', $K_2 =$ '$(\bar{1}6\bar{5}\bar{3})$' and $\eta_2 = [5\bar{1}\bar{4}3]$ where ' ' denotes approximations to irrational indices. As discussed, for example, by Christian [18] and Crocker [19], it was at one time thought to occur in deformation twinning of magnesium, but subsequently not [16], and has been shown to be in accord with the internal shears required to accommodate the b.c.c. to h.c.p. martensitic transformations in lithium, titanium and zirconium. We have therefore considered the dislocation for this mode, as defined in Table 1. The generally irrational nature of η_1 precludes simulation of the dislocation in the pure edge or screw orientations, since periodic boundary conditions are required in the line direction, and so the same $[1\bar{2}10]$ line direction as employed for the $\mathbf{b}_3$ and the $\mathbf{b}_4$ defects has been used. The $[1\bar{2}10]$ projection of this mixed dislocation is plotted in Fig. 3(c): η_1 is shown dashed because it is not in the plane of the paper. The Burgers vector $\mathbf{b}_2$ is given by the difference of the two lattice translation vectors shown and makes an angle of approx. 23° to the line: it is approx. $1/9[1\bar{3}21]$ for the c/a used here. (The changes in atomic symbols as the line is circuited arise because of its screw component.) The core is seen to be slightly less localised than that of the $\mathbf{b}_4$ dislocation, presumably because the shuffles are easier, but much less wide than the $\mathbf{b}_2$ core in the $(10\bar{1}2)$ interface.

Data for the energy and mobility of this $(10\bar{1}1)$ dislocation, which was induced to move by applying the appropriate combination of e_{xz} and e_{yz} shears, are given in Table 2. The results are entirely consistent with the preceding discussion regarding core width, line energy and ease of glide. Nevertheless, it is not clear why this mode. which our simulations suggest should propagate more easily than that associated with the $\mathbf{b}_4$ dislocation, has not been seen experimentally. Examination of the loading conditions and surface analyses used to determine the elements for $\{10\bar{1}1\}$ twinning in magnesium [16] and titanium [14, 17] indicates that the $\mathbf{b}_2$ mode would have been revealed had it occurred. This suggests that twin nucleation, rather than propagation, may be the mechanism which controls the $\{10\bar{1}1\}$ mode observed in practice. In this regard, the relatively high value of the twinning shear s for the $\mathbf{b}_2$ twin may be a crucial factor.

For completeness, we should quote the critical strains required to make dislocations glide in a single crystal defined by the na56 potential. Liang and Bacon [19] found by computer simulation that e_c is 0.001 for $\frac{1}{3}\langle 11\bar{2}0\rangle$ (0001) slip, 0.003 to 0.050 for $\frac{1}{3}\langle 11\bar{2}0\rangle$ $\{10\bar{1}0\}$ slip, and 0.015 for $\frac{1}{3}\langle 11\bar{2}3\rangle$ $\{10\bar{1}1\}$ and $\frac{1}{3}\langle 11\bar{2}3\rangle$ $\{11\bar{2}2\}$ slip. It should be noted, however, that slip was asymmetric on the $\{11\bar{2}2\}$ plane, and that under a resolved shear consistent with [0001] tension, the edge dislocation with $\mathbf{b} = \frac{1}{3}\langle 11\bar{2}3\rangle$ decomposed at $e_c = 0.015$ into a $\{11\bar{2}1\}$ twin, a result found earlier by Minonishi *et al.* [20] using a Lennard–Jones potential. The twin was observed to extend by the movement of steps one atomic plane in height, which is not surprising in view of the results of Section 4. More generally, the e_c values reported in Table 2 are seen not to be unreasonably high in comparison with the data from [19].

As remarked at the beginning, the results of this paper are based solely on the na56 pair potential, yet we know that the width of some of these cores is potential-dependent [6, 19]. However, the general trends in the differences between different dislocations are not so potential-specific, and the na56 function is believed to be the best available for an h.c.p. model. There are grounds, therefore, for guarded optimism that the results obtained have more general validity. This can only be decided for certain by carrying out simulations using more sophisticated procedures. To this end, we are now extending this research by employing many-body, embedded-atom potentials.

6. CONCLUSIONS

1. The properties of twinning dislocations in $\{10\bar{1}1\}$, $\{10\bar{1}2\}$, $\{11\bar{2}1\}$ and $\{11\bar{2}2\}$ twin boundaries have been have been investigated by computer simulation.

2. The core energy of these interfacial dislocations is primarily determined by the width of core spreading along the boundary. Very large variations in core width have been found.

3. The mobility of the dislocations is strongly dependent on core width.

4. The magnitude of the twinning shear does not determine the core energy and mobility.

5. The step height associated with twinning dislocations influences core width only in as much as it affects the amount of atomic shuffling which is associated with twinning.

6. The dislocation of lowest energy and highest mobility for $\{10\bar{1}1\}$ twinning does not correspond to the mode found in practice, suggesting that twin nucleation may be an important factor in this case.

7. Generally, however, our simulation results are found to be in good accord with the experimental features of twinning in h.c.p. metals.

Acknowledgements—This work was undertaken with the aid of a grant from the Acciones-Integradas programme of the British Council and the Spanish Government, and financial support of the Spanish CICYT project Mat 88-0496 and the University of Liverpool.

REFERENCES

1. M. H. Yoo, *Metall. Trans. A* **12,** 409 (1981).
2. P. G. Partridge, *Metall. Rev.* **118,** 169 (1967).
3. S. Mahajan and D. F. Williams, *Int. Metall. Rev.* **18,** 43 (1973).
4. A. G. Crocker and M. Bevis, in *The Science, Technology and Application of Titanium* (edited by R. Jaffe and N. Promisel), p. 453, Pergamon Press, Oxford (1970).
5. A. Serra and D. J. Bacon, *Phil. Mag. A* **54,** 793 (1986).
6. A. Serra, D. J. Bacon and R. C. Pond, *Acta metall.* **36,** 3183 (1988).
7. R. C. Pond, in *Dislocations and Properties of Real Materials*, p. 76. Inst. of Metals, London (1985).
8. V. Vitek, A. P. Sutton, D. A. Smith and R. C. Pond, in *Grain Boundary Structure and Kinetics* (edited by R. W. Baluffi), p. 115. Am. Soc. Metals, Ohio (1980).
9. R. C. Pond, D. J. Bacon, A. Serra and A. P. Sutton, *Metall. Trans.* In press.
10. D. J. Bacon, *J. nucl. Mater.* **159,** 176 (1988).
11. D. J. Bacon and M. H. Liang, *Phil. Mag. A* **53,** 163 (1986).
12. S. Hagège, M. Mori and Y. Ishida, *J. Physique.* To be published.
13. R. E. Reed-Hill, E. P. Dahlberg and W. A. Slippy, *Trans. Am. Inst. Min. Engrs.* **233,** 1766 (1965).
14. N. E. Paton and W. A. Backofen, *Metall. Trans.* **1,** 2839 (1970).
15. A. Akhtar, *J. nucl. Mater.* **47,** 79 (1973).
16. R. E. Reed-Hill, *Trans. Am. Inst. Min. Engrs* **218,** 554 (1960).
17. N. E. Paton and W. A. Backofen, *Trans. Am. Inst. Min. Engrs* **245,** 1369 (1969).
18. J. W. Christian, *Transformations in Metals and Alloys.* Pergamon Press, Oxford (1965).
19. A. G. Crocker, in *Deformation Twinning* (edited by R. E. Reed-Hill, J. P. Hirth and H. C. Rogers), p. 272. Gordon & Breach, New York (1964).
20. M. H. Liang and D. J. Bacon, *Phil. Mag.* **A53,** 205 (1986).
21. Y. Minonishi, S. Ishioka, M. Koiwa, S. Morozumi and M. Yamaguchi, *Phil. Mag.* **A45,** 835 (1982).